Nonperturbative treatment of single ionization of H_2 by fast highly-charged-ion impact

L. Sælen,[1,2] T. Birkeland,[3] N. Sisourat,[2,4] A. Dubois,[2,5] and J. P. Hansen[1]

[1]*Department of Physics and Technology, University of Bergen, N-5007 Bergen, Norway*

[2]*UPMC Univ. Paris 06, UMR 7614, Laboratoire de Chimie Physique-Matière et Rayonnement, F-75005 Paris, France*

[3]*Department of Mathematics, University of Bergen, N-5008 Bergen, Norway*

[4]*Theoretische Chemie, Universität Heidelberg, Im Neuenheimer Feld 229, D-69120 Heidelberg, Germany*

[5]*CNRS, UMR 7614, Laboratoire de Chimie Physique-Matière et Rayonnement, F-75005 Paris, France*

(Received 25 November 2009; published 22 February 2010)

We present a detailed analysis of the interference effects observed for ionization in collisions of fast highly charged projectiles with molecular hydrogen. We propose a nonperturbative semiclassical approach to describe the process under consideration by solving the time-dependent Schrödinger equation fully numerically on a 3D spatial grid. We present results for Kr^{34+}-H_2 collisions at 63 MeV/u impact energy and discuss different structures observed experimentally in doubly differential cross sections. The presence of Young-type minima and the absence of high-frequency oscillations are especially addressed. We also report unexpected interference patterns which can be observed for fixed-in-space molecular targets.

DOI: 10.1103/PhysRevA.81.022718 PACS number(s): 34.50.Gb

I. INTRODUCTION

The observation of the coherent emission of electrons by H_2 in the collisions with fast highly charged ions have been made possible through the continued improvements of experimental techniques which recently allowed for the recording of tiny variations in the ionization differential cross sections. By dividing the data obtained for H_2 with those calculated for the equivalent atomic target, Stolterfoht and collaborators [1,2] were able to show a clear interference pattern in the electron energy domain ranging from a few eV to about 300 eV where the cross sections drop by more than three orders of magnitude. The observed oscillation demonstrated the coherent electron emission from the H_2 target with the two nuclei acting as slits in analogy with Young's famous experiment in optics. In that context the H_2 target cannot be considered as two independent hydrogen atoms, in the way it is often used to evaluate cross sections for complex molecular targets [3].

Numerous experimental and theoretical investigations have confirmed and extended the outcomes of the 2001 publication, for example [4–9], and more recently [10,11]. Among others, two important features of the energy differential distributions have been the objects of multiple investigations: (i) the asymmetry of the cross sections in forward and backward electron emission which was only recently explained [10] and (ii) the presence of higher-frequency structures in the (Young-type) interference pattern. These interference structures, which were exhibited by dividing the cross-section ratio with a smooth oscillatory fit [6,12], were demonstrated to be weak (few percentages of the data), independent of the emission angle and interpreted as multiple scattering of the electronic outgoing waves. No theoretical model nor calculation has confirmed and explained such structures. This is a rather puzzling challenge since the same effect, though applied in an amplifying medium, is the source of an important experimental x-ray technique known as extended x-ray absorption fine structure (EXAFS) which uses multiscattering phenomena in order to scan the surroundings of the emitting atoms and obtain detailed structural informations in solids. The EXAFS spectra can be explained by the superposition of amplitudes and phase shifts related to multiple scattering paths with respect to the single scattering ones, cf. for example, Ref. [13].

In this article we investigate both topics based on an *ab initio* nonperturbative simulation of Kr^{34+}-H_2 collisions for a single velocity ($v = 50$ a.u. or, correspondingly, $E \approx 63$ MeV/u impact energy) which is within the range of most experimental studies. Our results stem from full 3D solutions of the time-dependent Schrödinger equation and serve as a direct extension of the work of Sisourat *et al.* [10] which focused on 1D and 2D models. Indeed, these models magnify interference effects at the cost of obvious physical drawbacks which makes direct comparisons with experimental data impossible. We present ejected electron energy and angle differential cross sections, as well as probability densities in momentum space, for different molecular orientations to illustrate the challenges raised. In particular we show that within the present computational accuracy we cannot see clear evidence of the multiple-scattering phenomena. However, another interference effect is demonstrated, where the electron is scattered from the projectile as well as the molecular (or atomic) target. This effect has been previously demonstrated in similar contexts for light ion impact at moderate velocities [11,14,15] by considering the scattering angle of the projectiles. In the following, atomic units will be used except where otherwise stated.

II. THEORETICAL MODEL AND NUMERICAL IMPLEMENTATION

A. Collision system and propagation scheme

To model the collisions between H_2 and highly charged ions the semiclassical approach is used, meaning that the projectile follows a classical trajectory expressed as $\vec{R}(t) = \vec{b} + \vec{v}t$, cf. Fig. 1. Moreover, the sudden approximation in which the two target nuclei are kept fixed during the collision is used since we focus our investigation on the high-impact energy range and on outgoing electron velocities ranging from about 1 to 6. In this context the time-dependent Schrödinger equation

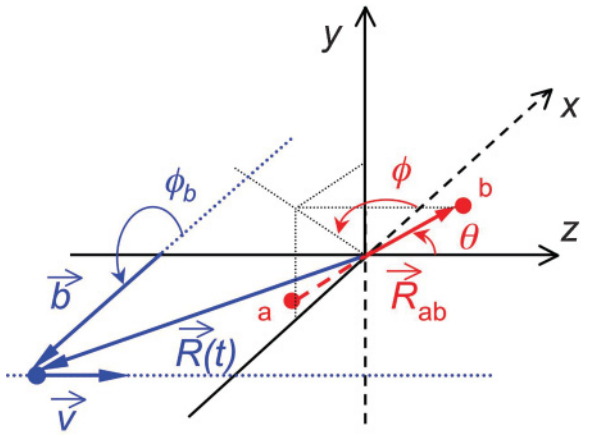

FIG. 1. (Color online) Schematic view of the collision geometry, showing the impact parameter $\vec{b}$ along the x direction, the projectile velocity, $\vec{v}$ along the z direction, the projectile-target internuclear vector $\vec{R}(t)$, and the molecular target internuclear vector $\vec{R}_{ab} = \vec{R}_b - \vec{R}_a$, whose orientation is given by $\Omega = (\theta, \phi)$. The azimuthal angle ϕ lies in the xy plane. In the analysis section, references will be made to detection at 0° and 180°, relating to electron detection along positive and negative z axis respectively, as well as 90°, corresponding to detection in the xy plane.

(TDSE),

$$\left[H_e - i\frac{\partial}{\partial t}\right]\Psi(\vec{r}, t) = 0, \tag{1}$$

is solved within the single-active-electron approximation, the electronic Hamiltonian H_e being expressed as

$$H_e = -\frac{1}{2}\nabla^2 - \frac{Z_p}{\sqrt{|\vec{R}(t) - \vec{r}|^2 + \beta^2}} - \frac{Z_H}{\sqrt{|\vec{R}_a - \vec{r}|^2 + \alpha^2}} - \frac{Z_H}{\sqrt{|\vec{R}_b - \vec{r}|^2 + \alpha^2}}. \tag{2}$$

Here Z_P is the projectile charge, $\vec{R}_a$ and $\vec{R}_b$ are the position vectors of the two target nuclei, and Z_H their charge. In our implementation we use regularized Coulomb soft-core potentials to avoid the singularity at the projectile nucleus. The target nuclei are effectively soften by the finite resolution of the grid.

A grid based treatment is used to represent the electronic wave function in which the space spanned by the active electron is discretized. A uniform 3D Cartesian grid has been employed. The TDSE is then solved by a split-step method [16] where the propagation of the initial wave function is performed by the symmetric Strang splitting scheme [17],

$$|\psi(t + \Delta t)\rangle = \mathcal{F}^{-1}\exp\left(-i\frac{1}{2}k^2\frac{\Delta t}{2}\right)\mathcal{F}\exp(-iV\Delta t) \times \mathcal{F}^{-1}\exp\left(-i\frac{1}{2}k^2\frac{\Delta t}{2}\right)\mathcal{F}|\psi(t)\rangle. \tag{3}$$

Here, V is the complete potential including the interaction between the active electron and the target and projectile nuclei, cf. Eq. (2). The highly efficient fast Fourier transform algorithm $\mathcal{F}$ is used to transform the wave function into momentum space where the Laplacian operator is diagonal.

In order to evaluate the (initial) ground state of the target as well as some of its lowest excited states, we have implemented the implicitly restarted Arnoldi method (IRAM) [18]. These states have been used to remove the bound part of the scattering wave function after the collision has taken place. This procedure was necessary because the plane waves employed as approximate continuum states are not orthogonal to the bound states of the system [19].

The wave function consumes a considerable amount of memory and an efficient parallelization scheme is required in order to get the results for a single propagation within a reasonable time scale (hours). As all elements in Eq. (3) apart from the Fourier transform operate independently on each grid point, the propagation scheme is well suited for distributed data parallelization. On the other hand, the data access pattern required for the Fourier transform is particularly ill suited for parallelization. We have therefore used the strategy described in Ref. [20]. It is based on the fact that a three-dimensional Fourier transform is equivalent to three one-dimensional Fourier transforms carried out in sequence. One or two dimensions of the wave function are distributed among the processors, and the Fourier transform is obtained by performing a sequence of 1D Fourier transforms on the processor local dimension, followed by a data redistribution to localize a different dimension.

All computations were performed using the PYPROP package [21] on the Cray XT4 system available at the University of Bergen. With the parallelization scheme and the grid and time parameters presented in the following we were able to obtain the results from a single collision in less than three hours using 512 cores.

B. Convergence tests

The results presented in the following are performed using a spatial grid in $q \in [-75, 75]$ discretized with $N = 1024$ grid points (with spacing $\Delta q \approx 0.15$) in each Cartesian dimension ($q \equiv x, y, z$). This grid size corresponds to a total of about 10^9 points, i.e., 16 GB of memory, and a significant increase of $q_{\max}$ or decrease of Δq was not possible with the computational resources at our disposal. We therefore performed thorough tests on the spacial grid parameters in two dimensions, concurring also with the results of Ref. [10].

Because of the limited extent of the grid, the parts of the ionized wave function with the highest momenta reach the grid boundary before the propagation is completed. We have therefore applied absorbing conditions so that the wave function is scaled every time step with the following absorber

$$1 - \cos^{80}\left(\frac{\pi}{2}(1 - |q|/q_{\max})\right). \tag{4}$$

This has the effect of smoothly scaling the wave function to zero at $q \approx q_{\max}$ and removing the fastest electrons as they reach the region near the boundaries, without significantly perturbing the inner part of the wave function.

Due to the memory requirements of the grid used for propagation, it was necessary to obtain the bound states on a smaller grid. This is justified by the fact that the spatial extension of these lowest excited states are far smaller than what is needed for propagating the collision. The discontinuity

originating from the use of two different box sizes was tested in two dimensions and it was found that indeed it introduced small, very high frequency oscillations (noise) in the results. These oscillations were smoothed out when convoluting the results and, more important, the procedure was found not to alter the significant structures of the results. The eigenstates are thus described on a grid of dimensions $q \in [-37.5, 37.5]$ with $N = 512$ grid points, keeping the same resolution as the propagation grid. The bound states were tested for stability by propagating them in time on the full grid without any external potential, which would have revealed any significant perturbation of the Hamiltonian due to the reduced box size. In order to separate the excited part of the wave function from the ionizing part, we have projected out the N_b lowest bound target states. By inspecting the decay of the population of these states after the collision, it was found that $N_b = 8$ is sufficient for convergent results.

To compare the cross sections for molecular target with those obtained for atomic target we have also calculated the hydrogenic eigenstates on the grid. This turned out to be very difficult due to the large degree of degeneracy, and a combination of approaches was necessary. We were able to obtain accurately converged states using the above approach for the $1s$, $2s$, and $3s$ states. These states were combined with the exact hydrogenic bound states evaluated on the grid in order to obtain the degenerate p and d states, completing the shell structure up to $n = 3$. The reason for not applying exact hydrogenic s states directly is due to the cusp at the origin for these states which makes them poorly represented in the Fourier basis.

Following the procedure described above and with the given grid resolution, we obtained the H_2 ground-state energy at -0.615 for $R_{ab} = 1.4$ and $Z_H = 0.636$. For comparison we used an atomic hydrogen target with an ionization energy of 0.495.

The time step that we have used in the computation presented below is $\Delta t = 0.006$ and was checked for convergence by propagating with considerably smaller time steps. The propagation time is set up by the initial and final projectile positions (z_i and z_f respectively) with respect to the target center of mass: we used $z_i = -100$ and $z_f = 400$ so that the propagation time was $T_{coll} = 10$. This allows the slow electrons to be far enough apart from the target ion so that the analysis of wave function can be considered accurate for such electrons.

Note finally that capture is extremely weak for the impact energy under consideration. The contribution of such processes is far below the absolute accuracy that we have been able to reach in our work.

C. Cross sections and collision setup

The last stage of the calculation is the analysis of the propagated wave function. We use the plane wave approximation in order to calculate emitted electron differential cross sections. As the bound states are not orthogonal to plane waves they must be projected out from the final wave function. This process gives rise to the so-called ionization wave function $\psi_{\rm ion}(\vec{r})$ and alternatively to its Fourier transform $\tilde{\psi}_{\rm ion}(\vec{k})$. Here, $\vec{k} = (k, \Omega_k)$ with $\Omega_k = (\theta_k, \phi_k)$ is the outgoing electron momentum, related to energy $\epsilon = \frac{1}{2}k^2$.

The use of plane waves in the analysis requires long propagation times to ensure that the outgoing electrons are far away from the nuclei. Due to the limitations in grid size, propagation for more than $T = 10$ in time would lead to significant absorption of the slow electrons at the boundary. To check that $T = 10$ is sufficient we interpolated the ionization wave function on a four times larger grid with correspondingly lower resolution and propagated this wave function for another $\Delta T_{coll} = 20$. We found mostly changes for the $k < 1$ electrons and no significant change in the results for $1 < k < 6$, an upper bound for our results, arising from the grid resolution and time steps used in the propagation.

We obtain the ionization wave function in position and momentum space, respectively $\psi_{\rm ion}(\vec{r}; b, \phi_b, \Omega)$ and $\tilde{\psi}_{\rm ion}(\vec{k}; b, \phi_b, \Omega)$, containing all information about the ionized electron. The parametric dependence includes molecular orientation Ω and impact parameter $\{b, \phi_b\}$, cf. Fig. 1. Assuming uniform ion beam and randomly oriented molecular target, the outgoing electron momentum-differential cross section is

$$\frac{d\sigma_{\rm ion}}{d\vec{k}} = \int_\Omega \left(\int_{\vec{b}} \frac{d\sigma_{\rm ion}}{d\vec{k} d\vec{b} d\Omega} \, b \, db d\phi_b \right) \sin\theta d\theta d\phi, \qquad (5)$$

where

$$\frac{d\sigma_{\rm ion}}{d\vec{k} d\vec{b} d\Omega} = \frac{1}{4\pi} |\tilde{\psi}_{\rm ion}(\vec{k}; b, \phi_b, \Omega)|^2 \equiv \frac{dD(\vec{k})}{d\vec{k}}. \qquad (6)$$

Consider the innermost integral in the expression above,

$$\int_0^{2\pi} |\tilde{\psi}_{\rm ion}(\vec{k}; b, \phi_b, \Omega)|^2 \, d\phi_b, \qquad (7)$$

and in particular detection in perpendicular and parallel directions. The first involves detection in a plane perpendicular to the trajectory of the projectile, and the latter involves detection along a single angle.

Perpendicular detection (90°). Transforming $\{k_x, k_y, 0\}$ to $\{k, \phi_k\}$ and integrating over ϕ_k, we find that the integrations over ϕ_b and ϕ are equivalent, where ϕ is the azimuthal molecular angle defined in Fig. 1. Thus, instead of integrating over ϕ_b, we may integrate over ϕ.

Parallel detection (0° and 180°). For parallel detection, $\vec{k}$ lies entirely along k_z. There is no integration over ϕ_k and we can directly interchange the ϕ_b integration with integration over ϕ. The integral over ϕ is done by a discrete sum as only a few molecular orientations are available (see below).

The evaluation of cross sections has been performed by collecting the results from the computations of seven different trajectories, namely $b \in \{0.5, 1, 2, 3, 5, 7, 10\}$, and four molecular target orientations, $(\theta, \phi) \in \{(0, 0), (\pi/2, 0), (\pi/2, \pi/2), (\pi/2, \pi/4)\}$. The three last orientations are all in a plane perpendicular to the ion beam, the last one being used to obtain the results for the symmetric configuration $(\pi/2, 3\pi/4)$, providing a fifth data point. Since the data points are not evenly distributed over the sphere, some weighting should be given to the different contributions in computing the integrations over Ω. This has been accomplished using Voronoi surfaces [22] which partitions the sphere into a set of regions, each corresponding to a vertex (data point). The regions are such

that all points in a region are closer to the vertex of that region than any other vertex. The area associated with each data point thus gives a cubature for approximating the integral over the sphere and can be used as a weight of that data point in the cross section evaluation (the total area being 4π). After organizing the terms, the integration over molecular orientations becomes a sum over two terms, with the factor 1.899 for the contribution from the parallel orientation and 1.096 for the perpendicular orientations. Note that there are several perpendicular orientations, but they all give identical contribution here due to the integration over ϕ_k and ϕ above.

The connection to the experimental energy cross section, $\frac{d\sigma_{\text{ion}}}{d\Omega_k d\epsilon}$, where $d\Omega_k$ and $d\epsilon$ refer to the solid angle and the energy of the outgoing electron, is simply given by the relation $k = \sqrt{2\epsilon}$ so that

$$\frac{d\sigma_{\text{ion}}}{d\Omega_k d\epsilon} = \frac{d\sigma_{\text{ion}}}{d\Omega_k k dk}. \tag{8}$$

Note that to compare with experiments and to remove the high-frequency noise stemming from the use of different grids for the stationary problem and the propagation, we have filtered the differential cross section through a low-pass filter (Gaussian convolution) with a half-width of 0.02, corresponding approximately to the experimental resolution in Ref. [2]. The cross sections at forward and backward emission angles give particularly low statistics. To compensate for this we have used the integrated probability densities instead of a single cut of the wave function at $k_x = k_y = 0$. Due to the extremely fast decay of the wave function with electron momentum, the integration effectively amounts to an average of data in a narrow cone around the forward and backward directions. This procedure is in fact in closer resemblance to a physical detector.

III. RESULTS AND DISCUSSION

In this section we present the results of our calculations performed on the 63 MeV/u Kr^{34+}-H_2 collision system compared with the experimental data reported in Ref. [2], where slightly different parameters (Z_p and v) were used.

In Fig. 2 we show this comparison at the level of the differential ionization cross sections as function of the outgoing electron energy. Reasonably good correspondence between experiments and calculations are observed. As noticed in the experimental investigations, the cross sections decay significantly faster for parallel detection compared with perpendicular detection, making the analysis of interference effects more challenging. We also predicted that the cross sections for backward emission ($\theta_k = 180°$) are significantly smaller than the ones for forward emission ($\theta_k = 0°$), in agreement with the 1D-2D results in Ref. [10] and the measurements reported in [23].

To magnify any interference effects, we show in Fig. 3 the ratio between cross sections for a molecular and an atomic hydrogen target. The solid line in the lower panel, describing the forward ($\theta_k = 0°$) ionization, shows a large valley at about 73 eV, i.e., a momentum $k \approx 2.3$. This is in good agreement with previously reported experimental and theoretical data and

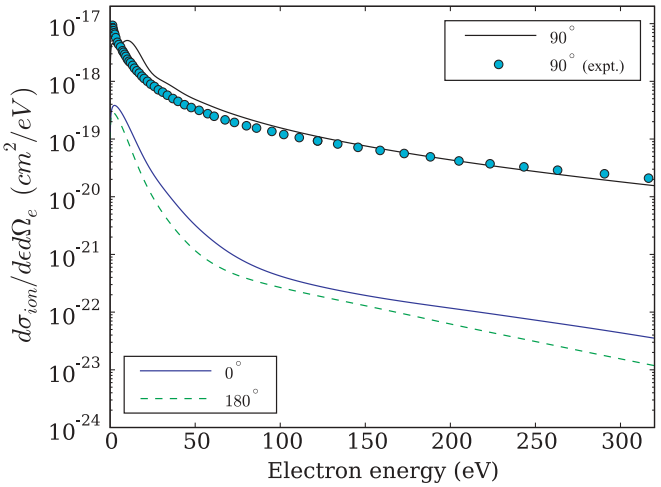

FIG. 2. (Color online) Differential ionization cross sections as a function of the ejected electron energy for 63 MeV/u collisions Kr^{34+}-H_2, obtained at the detection angles $\theta_k = 0°$ (lower solid line), 90° (upper solid line), and 180° (dashed line). The filled circles show the experimental results [2] obtained at 90°for Kr^{33+} at 68 MeV/u.

roughly follows the simple interference formula [10]

$$k = \frac{\pi}{R_{ab}}(2n+1), n = 0, 1, 2, 3, \ldots \tag{9}$$

which was also derived in the context of photoionization by Fernandez *et al.* [24].

From this, the position of the minima (destructive interference) of the cross sections can be obtained. Note that the present calculations are not converged for fast electrons (not presented in the figures), to be able to show the successive minima. Figure 3 displays a clear asymmetry in the ratio between forward and backward emission which is explained

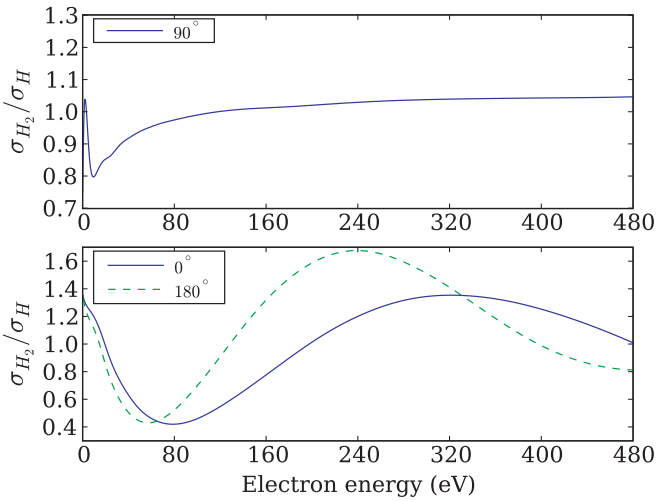

FIG. 3. (Color online) Ratio of the differential cross sections (marked as σ for simplicity) for H_2 with those for H as function of the outgoing electron energy. Upper panel displays perpendicular detection. Lower panel displays in solid line forward detection ($\theta_k = 0°$), and in dashed line backward detection ($\theta_k = 180°$).

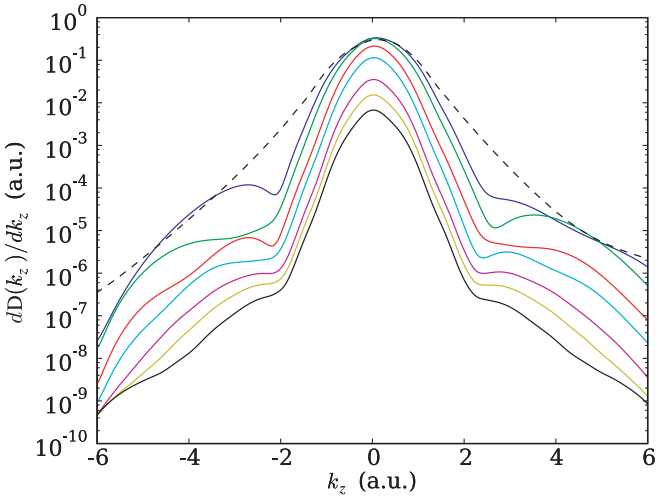

FIG. 4. (Color online) The probability density corresponding to the ionization wave function [cf. Eq. (6)] integrated over k_x and k_y as a function of the outgoing electron momentum k_z. The molecular target as well as the direction of detection are aligned parallel to the beam (z axis), k being set positive (negative) for forward (backward) detection. The seven solid curves correspond to the impact parameters $b = \{0.5, 1, 2, 3, 5, 7, 10\}$ ($\phi_b = 0$). The uppermost curve corresponds to lowest impact parameter, the overall probability density decreasing in magnitude with increasing b. The dashed line corresponds to the probability density for an atomic hydrogen target with impact parameter $b = 0.5$.

by a phase shift introduced to take into account the time delay for the projectile to initiate successive ionization at both nuclei [10]

$$\phi^{\pm}_{\rm ion}(x,t) \approx e^{\pm i|k|(x+\frac{R_{ab}}{2})-i\frac{k^2}{2}t} + e^{\pm i|k|(x-\frac{R_{ab}}{2})-i\frac{k^2}{2}(t-\delta t)}. \qquad (10)$$

The criterion for destructive interference is then given by

$$|k| \pm \frac{k^2}{2v} = \frac{(2n+1)\pi}{R_{\rm ab}}, \qquad (11)$$

with $+(-)$ for forward (backward) detection. This predicts minima located respectively at $k = 2.3, 7.3, \ldots$ $(72, 725, \ldots$ eV) in the forward direction and $2.2, 6.3, \ldots$ $(66, 540, \ldots$ eV) in the backward direction. Although this is a 1D model, we see an impressive agreement with the current results. However, compared to the 1D calculations [10], the minima display a much wider spread and are not as pronounced. This is understood by the integrations over impact parameters, azimuthal angles, and molecular orientations required to obtain the differential cross sections. To illustrate this difference, the dependence on impact parameter is investigated in the following.

Having the ionization wave function we are able to analyze each collision event in detail without averaging over the impact parameters, molecular orientations, and detection angles. In Fig. 4 we show the ionization probability density as function of outgoing electron momentum for seven impact parameters and for a configuration where both detection direction and molecular orientation are parallel to the projectile velocity. The Young-type first minima are clearly seen in the backward and forward directions for the molecular target (solid lines), while the data decay smoothly for the atomic target (dashed line). The uppermost solid curve corresponds to the smallest impact parameter, i.e., nearly head-on collision. In this case the forward/backward asymmetry for the first minimum is then maximum and their positions (-2.2 and 2.3 approximately) are in close agreement with the 1D model, Eq. (11). However, for increasing impact parameters the prediction obtained in the 1D model ($b = 0$) becomes inaccurate. As $b \gg R_{ab}$, the time difference for ionization to initiate on both nuclei becomes comparable to the overall interaction time so that the related phase shift in Eq. (11) is negligible. The asymmetry is indeed seen to decrease in Fig. 4 and hardly any asymmetry is observed for the lowest curve ($b = 10$), both minima being located at $k \approx \pm 2$ The dependence on impact parameter contributes to smear the location of the minima in the calculated cross sections. However, even in this figure we cannot detect a pattern originating from a multiscattering mechanism.

While there are clear first-order interference effects for the molecular to atomic cross-section ratio at forward and backward emission angles, the ratio for perpendicular emission seems void of interference effects (upper panel of Fig. 3). A closer look at the curve, however, reveals some faint structures which can be investigated by regarding the results at every impact parameter. Figure 5 shows the molecular-to-atomic-target probability density ratio for the impact parameters $b = \{0.5, 1, 2, 3, 5, 7\}$. We see clear oscillations characterized by frequencies increasing with the impact parameter. These oscillations are indeed quite surprising, as no higher-order Young-type interferences would display this behavior. It turns out that these structures can be attributed to a phenomenon already discussed in low-energy collisions [11,15]. During the short time of the collision, the highly charged ion projectile interacts strongly with the active electron of H_2, and the ionized wave function is effectively scattered off both projectile and

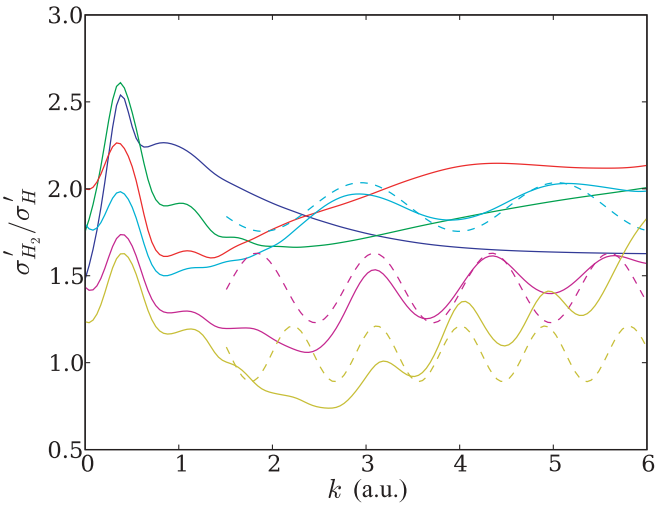

FIG. 5. (Color online) The molecular-to-atomic ratio of the probability densities [Eq. (6) integrated over ϕ_k and ϕ_b, marked σ' for simplicity] evaluated at $\theta_k = \pi/2$ for six different impact parameters $b = \{0.5, 1, 2, 3, 5, 7\}$. For H_2 target the internuclear axis is aligned perpendicular to the ion beam $\theta = \pi/2$. The solid lines follow the same color code as in Fig. 4. The dashed line correspond to sine fits commented in the text.

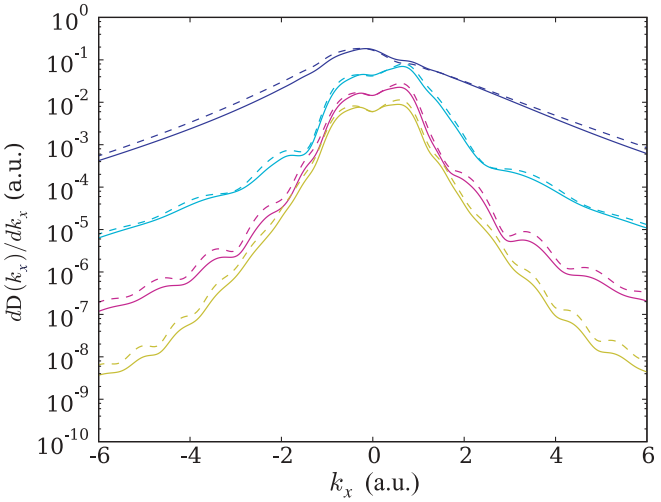

FIG. 6. (Color online) The probability density corresponding to the ionization wave function [cf. Eq. (6)] integrated over k_y and k_z as function of the electron momentum k_x. The densities are shown for molecular (solid lines) and atomic (dashed lines) hydrogen target at four impact parameters, $b = \{0.5, 3, 5, 7\}$ and $\phi_b = 0$. As before the uppermost curve corresponds to smallest impact parameter. The molecular target is aligned perpendicular to the z axis, $\Omega = (\pi/2, \pi/2)$.

target, giving rise to interference patterns in the electron spectrum.

It is possible to predict the b-dependent frequency by considering a simplified scenario of the ionization process. Ionization mainly occurs when the projectile is closest to the target, regardless of the molecular alignment. Consider the interference effect from two waves scattered at sites $x = 0$ (target center of mass position) and $x = b$ (projectile position at the closest approach). The different amplitudes will not give complete destructive interferences when the waves are added coherently, but will rather show oscillations whose minima are separated by $2\pi/b$ [cf. Eq. (9)]. In Fig. 5 we have also plotted the function $a_0 + a_1 \sin(kb/2\pi + \delta)$ for $b = 3, 5, 7$. The correspondence is striking, but naturally this simple model breaks down for impact parameters smaller than the internuclear distance. The picture we have presented implies two important features. First, the effect should be present for both atomic and molecular targets. Second, the effect should be dominant in the direction of the impact parameter (the x direction in Fig. 1). For that reason we show in Fig. 6 the probability densities in the x direction for the ionized wave function as a function of outgoing electron momentum. The molecular results are shown with solid lines for the impact parameters $\{0.5, 3, 5, 7\}$ and a molecule aligned along the y axis. The results for a hydrogenic target are shown with dashed lines for the same impact parameters. We observe identical oscillatory pattern for both targets, with decreasing frequency for smaller b. These structures are hardly detectable in the relative differential cross sections (Fig. 3) due to the integration over b. However, they could possibly be observed experimentally by measurements performed differentially with respect to the projectile scattering angle and with fixed-in-space molecular targets.

Finally, none of our results show higher-order frequency oscillations. However, our model is nonperturbative and should therefore includes all necessary mechanisms. Experimental work do show structures independent of the detection angle, and the EXAFS spectroscopy is related to such multiscattering processes which should be at least weakly present in our specific target conditions. The following gives an explanation of such absence.

The clear evidence of Young-type interferences do support the idea of electron emission initiated independently from small volumes close to both nuclei [25–27]. In this picture the further scattering of the outgoing electronic waves from one center by the other one, in the direction of the primary wave, can be compared to the elastic collisions of slow electrons by a hydrogen atom. However, this process is strongly selective in favor of forward scattering, the backward one being at least two orders of magnitude lower in this range of velocities [28]. The same, though weaker, selectivity appears for the primary process of ion-induced ionization. Three features can be inferred by these characteristics: (i) the signature of the interference between the direct and re-scattered waves should be of very small magnitudes, largely less that 1%; (ii) the magnitude of the oscillations should be different between forward and backward electron emission (the latter ones requiring two backscattering events); (iii) the magnitude of the oscillations should be decreasing for increasing electron velocities. Therefore the weak signatures of such higher-order interferences add to the difficulty of observing them in calculations. The numerical demonstration of their existence is out of reach at the present time.

IV. CONCLUSION

In conclusion we have presented a nonperturbative treatment to describe the ionization process during fast collisions between a highly charged projectile and molecular hydrogen target. Since based on a close-coupling approach, it takes into account all possible processes and mechanisms in the dynamical stage, except for electronic correlation and coupling between electronic and nuclear degrees of freedom which does not play a significant role in the processes under investigation. Our calculations show clear oscillatory structures and asymmetries in differential cross sections which are interpreted on a basis of only first-order interference effects, as in the Young's famous experiment in optics. Further experimental investigations, including detection of electrons and recoil ions in coincidence, will be very valuable to support the present predictions and interpretations.

ACKNOWLEDGMENTS

This research has been supported by the Research Council of Norway (RCN). L.S. was supported by a Eiffel Excellence Grant during her stay at UPMC and has received travel support from the Conseil Régional d'Ile-de-France within the SETCI program. We would like to thank Dr. Raymond Nepstad for useful discussions.

[1] N. Stolterfoht, B. Sulik, V. Hoffmann, B. Skogvall, J. Y. Chesnel, J. Rangama, F. Frémont, D. Hennecart, A. Cassimi, X. Husson *et al.*, Phys. Rev. Lett. **87**, 023201 (2001).

[2] N. Stolterfoht, B. Sulik, L. Gulyás, B. Skogvall, J. Y. Chesnel, F. Frémont, D. Hennecart, A. Cassimi, L. Adoui, S. Hossain *et al.*, Phys. Rev. A **67**, 030702(R) (2003).

[3] M. P. Gaigeot, R. Vuilleumier, C. Stia, M. E. Galassi, R. Rivarola, B. Gervais, and M. F. Politis, J. Phys. B **40**, 1 (2007).

[4] L. Nagy, L. Kocbach, K. Pora, and J. P. Hansen, J. Phys. B **35**, L453 (2002).

[5] M. E. Galassi, R. D. Rivarola, P. D. Fainstein, and N. Stolterfoht, Phys. Rev. A **66**, 052705 (2002).

[6] N. Stolterfoht, B. Sulik, B. Skogvall, J. Y. Chesnel, F. Frémont, D. Hennecart, A. Cassimi, L. Adoui, S. Hossain, and J. A. Tanis, Phys. Rev. A **69**, 012701 (2004).

[7] D. Misra, U. Kadhane, Y. P. Singh, L. C. Tribedi, P. D. Fainstein, and P. Richard, Phys. Rev. Lett. **92**, 153201 (2004), see also Comment and Reply.

[8] J. A. Tanis, S. Hossain, B. Sulik, and N. Stolterfoht, Phys. Rev. Lett. **95**, 079301 (2005).

[9] J. A. Tanis, J.-Y. Chesnel, B. Sulik, B. Skogvall, P. Sobocinski, A. Cassimi, J.-P. Grandin, L. Adoui, D. Hennecart, and N. Stolterfoht, Phys. Rev. A **74**, 022707 (2006).

[10] N. Sisourat, J. Caillat, A. Dubois, and P. D. Fainstein, Phys. Rev. A **76**, 012718 (2007).

[11] J. S. Alexander, A. C. Laforge, A. Hasan, Z. S. Machavariani, M. F. Ciappina, R. D. Rivarola, D. H. Madison, and M. Schulz, Phys. Rev. A **78**, 060701(R) (2008).

[12] S. Hossain, A. L. Landers, N. Stolterfoht, and J. A. Tanis, Phys. Rev. A **72**, 010701(R) (2005).

[13] P. A. Lee and J. B. Pendry, Phys. Rev. B **11**, 2795 (1975).

[14] L. Gulyàs, P. D. Fainstein, and T. Shirai, J. Phys. B **34**, 1473 (2001).

[15] F. Frémont, A. Hajaji, A. Naja, C. Leclercq, J. Soret, J. A. Tanis, B. Sulik, and J.-Y. Chesnel, Phys. Rev. A **72**, 050704(R) (2005).

[16] M. Feit, J. Fleck Jr., and A. Steiger, J. Comput. Phys. **47**, 412 (1982).

[17] G. Strang, J. Num. Anal. **5**, 506 (1968).

[18] D. C. Sorensen, SIAM J. Matrix Anal. Appl. **13**, 357 (1992).

[19] L. B. Madsen, L. A. A. Nikolopoulos, T. K. Kjeldsen, and J. Fernández, Phys. Rev. A **76**, 063407 (2007).

[20] T. Birkeland and T. Sørevik, in *Advances in Parallel Computing*, edited by C. Bischof, M. Bücker, P. Gibbon, G. R. Joubert, T. Lippert, B. Mohr, and F. Peters (IOS Press, Amsterdam, 2008), Vol. 15, p. 433.

[21] T. Birkeland and R. Nepstad, PYPROP—A Framework for Propagating the Time Dependent Schrödinger Equation, http://pyprop.googlecode.com.

[22] R. J. Renka, ACM T. Math. Software **23**, 416 (1997).

[23] D. Misra, A. Kelkar, U. Kadhane, A. Kumar, L. C. Tribedi, and P. D. Fainstein, Phys. Rev. A **74**, 060701(R) (2006).

[24] J. Fernández, O. Fojón, A. Palacios, and F. Martín, Phys. Rev. Lett. **98**, 043005 (2007).

[25] It should be remarked that the equivalence between the present system and the emission from two separate slits is quite surprizing, since in opposition with the concept of chemical bonds based on the sharing of the valence electrons between the nuclei (or cores). The interference effects have also been observed in K-shell photoionization of N_2 [26,27] where the initial location of the outgoing electrons close to the nuclei is unquestionable and the interference signature is indeed clearer in these cases.

[26] D. Rolles, M. Braune, S. Cvejanović, O. Geßner, R. Hentges, S. Korica, B. Langer, T. Lischke, G. Prümper, A. Reinköster, J. Viefhaus, B. Zimmermann, V. McKoy, and U. Becker, Nature **437**, 711 (2005).

[27] X. J. Liu, N. A. Cherepkov, S. K. Semenov, V. Kimberg, F. Gel'mukhanov, G. Prumper, T. Lischke, T. Tanaka, M. Hoshino, H. Tanaka, and K. Ueda, J. Phys. B **39**, 4801 (2006).

[28] I. Bray, D. A. Konovalov, and I. E. McCarthy, Phys. Rev. A **44**, 5586 (1991).